

# Measurement and Modeling of Normal Contact Stiffness and Contact Damping at the Meso Scale

Xi Shi

Andreas A. Polycarpou\*

e-mail: polycarp@uiuc.edu

Department of Mechanical and Industrial  
Engineering,  
University of Illinois at Urbana-Champaign,  
Urbana, Illinois 61801

*Modeling of contact interfaces that inherently include roughness such as joints, clamping devices, and robotic contacts, is very important in many engineering applications. Accurate modeling of such devices requires knowledge of contact parameters such as contact stiffness and contact damping, which are not readily available. In this paper, an experimental method based on contact resonance is developed to extract the contact parameters of realistic rough surfaces under lightly loaded conditions. Both Hertzian spherical contacts and flat rough surfaces in contact under normal loads of up to 1000 mN were studied. Due to roughness, measured contact stiffness values are significantly lower than theoretical values predicted from smooth surfaces in contact. Also, the measured values favorably compare with theoretical values based on both Hertzian and rough contact surfaces. Contact damping ratio values were found to decrease with increasing contact load for both Hertzian and flat surfaces. Furthermore, Hertzian contacts have larger damping compared to rough flat surfaces, which also agrees with the literature. The presence of minute amount of lubricant and wear debris at the interface was also investigated. It was found that both lubricant and wear debris decrease the contact stiffness significantly though only the lubricant significantly increases the damping. [DOI: 10.1115/1.1857920]*

## 1 Introduction and Background

Interfacial parameters including contact stiffness and contact damping are of great importance to contact dynamics and interface modeling. There are numerous applications where characterizing and understanding the interfacial behavior of lightly loaded contacts is critical. These include meso-scale assembling applications [1], robotic applications [2], grippers [3], micro-bearings and spindle bearings in magnetic storage hard disk drives [4], and lightly loaded mechanical joints in general. In all these cases, the contact loads involved range from a few millinewtons to hundreds of millinewtons. Joints and contacting surfaces provide coupling forces and moments between structures, as well as energy dissipation. Although joints and contacts are common in practical engineering applications, there are certain aspects of their dynamics such as sensitivity to interfacial parameters (e.g., contact stiffness, contact damping, and surface roughness) that are not fully understood and modeled. Such phenomena cause uncertainty in system performance and reliability predictions.

It is long known that treating surfaces as rigid bodies or as deformable solids without roughness is inadequate as practical surfaces always possess some degree of roughness. The simpler method to model a contact interface is to use a spring and a viscous damper in parallel. In such models, it is acknowledged that in the absence of lubricant at the interface, damping is very low, and also the stiffness is nonlinear with the normal load. More advanced models for contacting interfaces have also been suggested, where the stiffness from the asperities is separated from the stiffness of the lubricant [5], or the bulk stiffness is also added [6]. The contact stiffness can be obtained from analytical contact models, e.g., using the Hertzian contact model for spherical contacts [7]. For the case of rough surfaces in contact, the Greenwood

and Williamson (GW) [8] statistical model of rough surfaces is usually used to obtain the contact stiffness. Experimental measurements of such parameters are scarce as they are not readily obtained. In limited cases studied before, they are usually extracted using indirect methods [9] or system identification methods [10]. Descriptions of some of the methods which can measure interfacial parameters are discussed next.

Serpe [11] developed a tester to measure the contact stiffness of rough surfaces at the macro scale using the contact resonance method. The load range they studied was high, varying from 15 to 225 N. They measured very large contact stiffness values that increase with load, which also were in agreement with modeling results based on rough surfaces. Using a similar idea, Hess and Wagh [12] extracted the surface roughness from contact resonance measurements. Such works for measuring contact stiffness and contact damping are indirect methods. They all measure some parameters which are related to the contact stiffness and/or contact damping through some known dynamic system model. The key in such works is to know precisely the system dynamics under the conditions to be studied. Once such parameters are measured, the contact stiffness and/or contact damping can readily be obtained based on the known dynamic model.

A completely different method to measure contact stiffness is based on ultrasonic methods. According to Dwyer-Joyce and co-workers [13,14], if an interface is modeled as a stiff spring, an equation can be derived which predicts the frequency profile of the reflected ultrasound. By performing a Fourier transform upon the ultrasonic echo from the interface, the stiffness of that interface can be calculated. In their model, because the interfacial dynamics are modeled without considering the contact damping, they can only measure the contact stiffness.

Another method to measure contact stiffness and damping at the nano-scales has been presented by Asif et al. [15]. This method uses a "hybrid" nanoindenter instrument that is capable of depth-sensing nanoindentation and scanning probe imaging. A very sharp tip with sub-micron tip radius scans the surface using a

\*Corresponding author.

Contributed by the Technical Committee on Vibration and Sound for publication in the JOURNAL OF VIBRATION AND ACOUSTICS. Manuscript received September 1, 2003; final revision, February 6, 2004. Review conducted by L. Bergman.

sinusoidal load in the micronewton range. Then, using a dynamic model of the indenter, a map of complex stiffness is created. Although this imaging method is capable of very high sensitivity, the test rig is complicated and the dynamic model contains many uncertainties (nonlinearities).

A direct method based on the definition of the contact stiffness has also been used to extract contact stiffness values at the nano-scale. In such methods, one measures the contact load and the corresponding approach, and then from the slope, the contact stiffness is extracted directly. This idea has been successfully applied to nanoindentation measurements [16,17] to directly measure the contact stiffness. Although this method can achieve a very high sensitivity, it is only suitable in nano-scale applications and also it cannot measure the contact damping.

In this paper, a tester based on the resonant frequency method is developed. This tester can measure both contact stiffness and contact damping in meso scale interfaces. The contact load is varied from 100 to 1000 mN. The tester has a very simple dynamic response, so that the contact stiffness and damping can unambiguously be obtained. Both Hertzian and flat surfaces are tested under unlubricated dry conditions, and in the presence of minute amounts of lubricant and wear debris. In typical tests, the system resonance will be constant independent of the load, whereas the contact resonant frequency will shift with increasing contact load. The measured contact stiffness for both Hertzian and flat rough surfaces is favorably compared with modeled predictions.

## 2 Analytical Calculations of Contact Stiffness

**2.1 Concentrated Hertzian Contacts.** Hertzian contacts consisting of spherical surfaces are found in many practical applications, such as bearings, rail wheels, and clamping devices. Figures 1(a) and 1(b) show a schematic representation of an equivalent sphere of radius  $R$  in contact with a smooth surface and in contact with a rough surface, respectively. According to Hertzian contact theory, for a smooth sphere in contact with a smooth flat surface under a load  $P$ , the normal approach or deflection  $\Delta$  is given by [7]

$$\Delta = \left\{ \frac{9P^2}{16RE^*2} \right\}^{1/3} \quad (1)$$

where  $E^*$  is the equivalent Young's modulus of elasticity given by

$$\frac{1}{E^*} = \frac{1-\nu_1^2}{E_1} + \frac{1-\nu_2^2}{E_2}$$

subscripts 1 and 2 refer to surfaces 1 and 2, respectively. Differentiating the approach  $\Delta$  with respect to load  $P$  and taking the inverse yields the contact stiffness, i.e.

$$k_{CH} = \frac{dP}{d\Delta} = \frac{3}{2} \left( \frac{16RE^*2}{9} \right)^{1/3} P^{1/3} \quad (2)$$

Equation (2) gives the contact stiffness for a smooth Hertzian contact. However, it is well recognized that all engineering surfaces possess some degree of roughness, irrespective of how

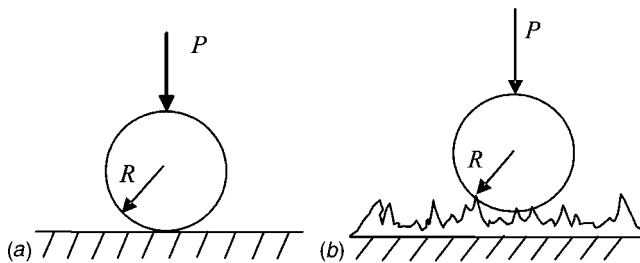


**Fig. 1 Schematic of a Hertzian contact: (a) smooth interface, (b) rough interface**

**Table 1 Typical CLA ( $R_a$ ) values from various manufacturing processes**

	Rough casting	Coarse machining	Fine machining	Grinding/polishing	Lapping/superfinishing
$R_a$ ( $\mu\text{m}$ )	10	3–10	1–3	0.2–1	0.02–0.4

smooth they are. For example fine machining operations produce surfaces with (rms) roughness values of  $R_q \approx 1 \mu\text{m}$ , where lapping and super-finishing produce much smoother surface with  $R_q \approx 0.1 \mu\text{m}$ . Table 1 lists typical roughness values that were obtained from different machining processes [18]. Typical values range from 0.02 to 10  $\mu\text{m}$  and one should expect that the degree of roughness will directly affect the contact stiffness.

Greenwood and Tripp [19] analyzed the contact between a rough sphere and a plane and reported that at low loads, the actual contact pressure in the presence of roughness is only one-third of the theoretical smooth Hertzian contact pressure. Consequently, the actual Hertzian contact stiffness in the presence of roughness at light loads will be approximately one-third of the value given by Eq. (2), i.e.

$$k_{CHR} = \frac{k_{CH}}{3} \quad (3)$$

At intermediate and higher loads,  $k_{CHR}$  is more complicated to calculate [19]. However, it is larger than that given by Eq. (3) and lower than that given by Eq. (2), since  $k_{CH}$  values based on smooth surfaces will give an upper-bound estimate.

## 2.2 Extended Flat Surfaces in Contact

**2.2.1 Smooth Surfaces.** When two flat surfaces are in contact, a simplification is to assume that they are infinity smooth, i.e., do not possess roughness. In the case of the contact between an infinitely smooth surface, which has thickness  $d_{th}$  and radius  $a$ , and a rigid infinite half space, shown in Fig 2(a), the relationship between the contact load  $P$  and the approach is given by [7]

$$\Delta = P \left( \frac{1-\nu^2}{\pi E^*} \right) \left[ 2 \ln \left( \frac{2d_{th}}{a} \right) - \frac{\nu}{1-\nu} \right] \quad (4)$$

Based on Eq. (4), the contact stiffness for smooth solids can readily be calculated and typical values for metallic surfaces are of the order of 10 GN/m, which are unrealistically high. As described in the next section, the presence of surface roughness decreases the values of the contact stiffness by several orders of magnitude.

**2.2.2 Rough Surfaces.** Greenwood and Williamson [8] introduced a systematic way of modeling surface roughness in contact, known as the GW model. In this model, it is assumed that the asperities on the surface are spherical in shape with a constant radius  $R_s$ , and the heights of the asperities follow a certain probability distribution function. Furthermore, they found that many engineering rough surfaces follow a Gaussian distribution. Figures 2(b) and 2(c) show a schematic representation of two contacting rough surfaces and the corresponding GW model, respectively. Assuming that under normal load all asperities deform elastically, the contact load is given by

$$P(d) = \frac{4}{3} \eta A_n E^* R_s^{1/2} \int_d^\infty (z-d)^{3/2} \phi(z) dz \quad (5)$$

where  $\phi(z)$  is the asperity height distribution. Following the same assumptions as in the original GW model, CEB [20] derived an elastic-plastic contact model. Assuming a Gaussian distribution for the asperity heights, the CEB model is given by

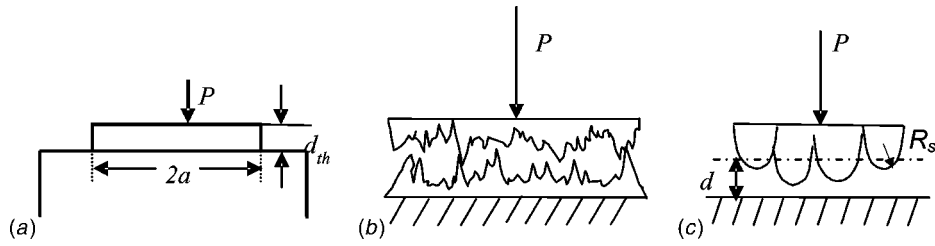


Fig. 2 (a) Infinitely smooth surfaces in contact; (b) rough flat surfaces in contact; (c) GW contact model

$$P(d) = \frac{4}{3\sqrt{2}\pi} \eta A_n E^* R_s^{1/2} \int_d^{d+\Omega_c} (z-d)^{3/2} e^{-z^2/2} dz + \sqrt{\frac{\pi}{2}} R_s K H \eta A_n \int_{d+\Omega_c}^{\infty} [2(z-d) - \Omega_c] e^{-z^2/2} dz \quad (6)$$

For a Gaussian distribution, there is no closed-form solution for the contact load  $P$ , for both elastic contact [Eq. (5)] and elastic/plastic contact [Eq. (6)], and thus the contact stiffness  $k_c$ . Therefore, the contact stiffness is calculated numerically based on Eq. (5) or (6). However, a good approximation to the Gaussian distribution is the use of an exponential asperity height distribution,  $\phi = c e^{-\lambda d/R_q}$  [21]. In this case, the contact calculations are simplified and there is a closed form solution to Eq. (5). Thus, for an exponential distribution and elastic contact, the nonlinear contact force is given by

$$P(d) = \frac{c \sqrt{\pi} \beta E^* A_n}{\lambda^{5/2}} \left( \frac{R_q}{R_s} \right)^{1/2} e^{-\lambda d/R_q} \quad (7)$$

where  $c = 17$  and  $\lambda = 3$  are curved-fitted constants that cover most practical ranges [21]. The contact stiffness is then obtained as

$$|k_c(d)| = \left| \frac{\lambda}{R_q} P(d) \right| \quad (8)$$

Equation (8), which gives the contact stiffness for the simpler case of elastically deformed asperities with an exponential distribution of asperity heights, implies that for a particular surface pair, the contact stiffness depends on the rms roughness  $R_q$  and the normal contact force.

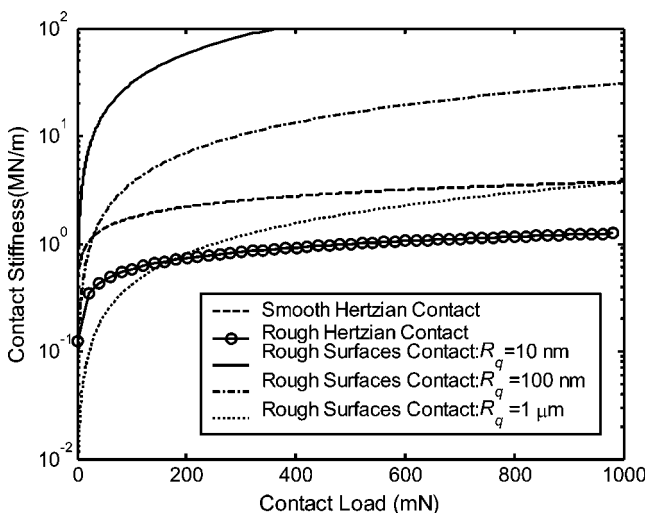


Fig. 3 Analytical contact stiffness versus contact load

**2.3 Contact Stiffness Simulations.** In order to gain further insight into the contact stiffness values for the different geometries discussed earlier, consider Fig. 3, which shows analytical contact stiffness predictions for Hertzian and rough surface contacts. For the Hertzian contact, the parameters used in the simulation are the same as listed in Table 2. For the rough surfaces in contact, the rms roughness used are  $R_q = 10$  nm, 100 nm, and 1  $\mu\text{m}$ , while all other parameters are the same as listed in Table 4. It is seen that in all cases, the contact stiffness is lower at low loads and initially increases sharply with load. For the Hertzian cases, the contact stiffness remains approximately constant after 100 mN, whereas for flat surfaces, the stiffness continuously increases with load. Furthermore, smoother surfaces have higher contact stiffness values than rougher surfaces. When, the surfaces are very rough with  $R_q = 1$   $\mu\text{m}$ , then the contact stiffness approaches that of Hertzian contacts. For example, at a contact load of 50 mN, the contact stiffness for rough surfaces with roughness  $R_q = 10$  nm,  $R_q = 100$  nm,  $R_q = 1$   $\mu\text{m}$ , smooth Hertzian and rough Hertzian ( $R = 0.794$  mm) is 17, 2, 0.2, 1.3, 0.43 MN/m, respectively, whereas at a much higher load of 1000 mN, their corresponding values increase to 220, 30, 3.6, 3.6, 1.2 MN/m. Despite the two to three orders of magnitude difference in contact stiffness values for the cases considered in Fig. 3, these values are still several orders of magnitude lower than the case of infinitely smooth flat surface in contact with a rigid infinite half space. In that case, for  $E^* = 105.3$  GPa,  $\nu = 0.29$ ,  $d_{th} = 10$  mm, and contact radius of  $a = 0.76$  mm, the theoretical contact stiffness  $k_c = 58.9$  GN/m, which is unrealistically high.

### 3 Experiment

**3.1 Experimental Tester.** Based on the theoretical contact stiffness predictions discussed in Sec. 2, values can vary by as much as several orders of magnitude depending on the contact geometry, the degree of roughness, and the normal load. Furthermore, the absence of models for contact damping makes experimental measurements of both of these quantities very important. As discussed in Sec. 1, an experimental method based on resonance is used in this work to measure the interfacial contact stiffness and damping. Figures 4(a) and 4(b) depict a schematic of the experimental tester and its system model representation, respectively. The contact interface is modeled as a linear stiff spring in parallel with a linear damping term. Because this experimental method is based on the contact resonant frequency, a critical part of the setup is to reliably obtain the true value of the contact resonance. Thus, a major issue in designing the tester is to isolate the contact elements from the other parts of the tester. In this research, two stainless steel soft tube springs ( $k_1, k_2$ ) are used to isolate the contact part from the tester frame. The dimensions of the tube springs are: diameter, 19 mm; length, 30 mm; and thickness, 0.5 mm. These dimensions are selected so that the system resonance will be low of the order of a few hundred hertz. Similarly,  $m_1 = 0.107$  kg and  $m_2 = 0.108$  kg are designed so that the value of the contact resonance is well above the system resonance but well below the structural tester resonances. The applied con-

**Table 2 Material and roughness parameters, Hertzian contact**

	Young's modulus $E$ (GPa)	Hardness $H$ (GPa)	Poisson ratio $\nu$	Radius $R$ ( $\mu\text{m}$ )	Roughness $R_q$ ( $\mu\text{m}$ )	Combined $E^*$ (GPa)	Combined $R$ ( $\mu\text{m}$ )
1/16 sphere stainless steel type 302	192.92	2.96	0.29	793.75	0.451	105.3	739.75
Flat sample 17-4PH stainless steel	192.92	2.96	0.29	...	0.137		

tact force is measured using strain gauges that are directly attached to the lower tube spring. Notice that the choice of ready-made force transducers (strain gauge-based or piezo-based) is prohibitive as it will add dynamic complexity to the system, by introducing additional frequencies in the range of interest.

**3.2 Strain Gauge Calibration.** In these experiments, the contact load was measured using miniature strain gauges attached directly on the outside surface of the lower tube spring shown in Fig. 4(a). Even though the experiments were performed in a laboratory room with controlled temperature (22°C) and humidity levels (25% RH), there was a small drift of the strain gage voltage signal. To minimize its effect on the measured load, calibrations were performed before and after each experiment. Such typical calibration curve is depicted in Fig. 5. It is observed that the calibration curve is very linear within the load range of interest and is almost identical before and after the experiment with a sensitivity of 0.042 mV/mN.

**3.3 Experimental Procedure.** The samples to be tested are attached on the top mass  $m_1$  and bottom mass  $m_2$  using rigid connections (set screws) to avoid introducing additional compliance in the system. A micrometer is used to exert the load by controlling the vertical position of the top mass. Once the surfaces come to contact under certain controlled contact load (determined from the strain-gauge readout), the vertical position of the top mass is locked in place, thus isolating the nonlinear and unknown dynamics of the micrometer. Then, an impact is exerted on the top

mass using a sharp impactor with a diameter of 0.8 mm and a weight of 2 mN. Conventional miniature accelerometers are attached on the lower mass to measure the accelerations of the mass block. To ensure that during an impact experiment there is no swing or rotation motion in the system, two accelerometers are attached on two opposite sides of the mass block. Monitoring the initial few milliseconds of data, to be identical from both accelerometers, ensures that there is no rotation of the mass. A typical measured acceleration response under an impact excitation is shown in Fig. 6(a). Notice that in all experiments performed in this work, the maximum acceleration remained under  $9.81 \text{ m/s}^2$  (1 g) ensuring that no loss of contact at the interface occurred. Figure 6(b) depicts average spectra (each spectrum is averaged from eight individual tests) obtained from three separate experiments under different normal loading conditions and using the same interface samples. As expected the system resonance is lower and approximately constant at 335 Hz, independent of load for the given cases. On the other hand, the contact resonance increases with increasing load, from 1880 to 2170 Hz for 440 and 800 mN, respectively. Note that there are no other resonances up to 10,000 Hz, confirming that the tester only contains the two desired resonances. The contact resonance is related directly to the contact stiffness and contact damping as described in the next section.

**3.4 System Dynamic Model.** Based on the lumped parameter system model shown in Fig. 4(b), the system dynamic equations can be written as

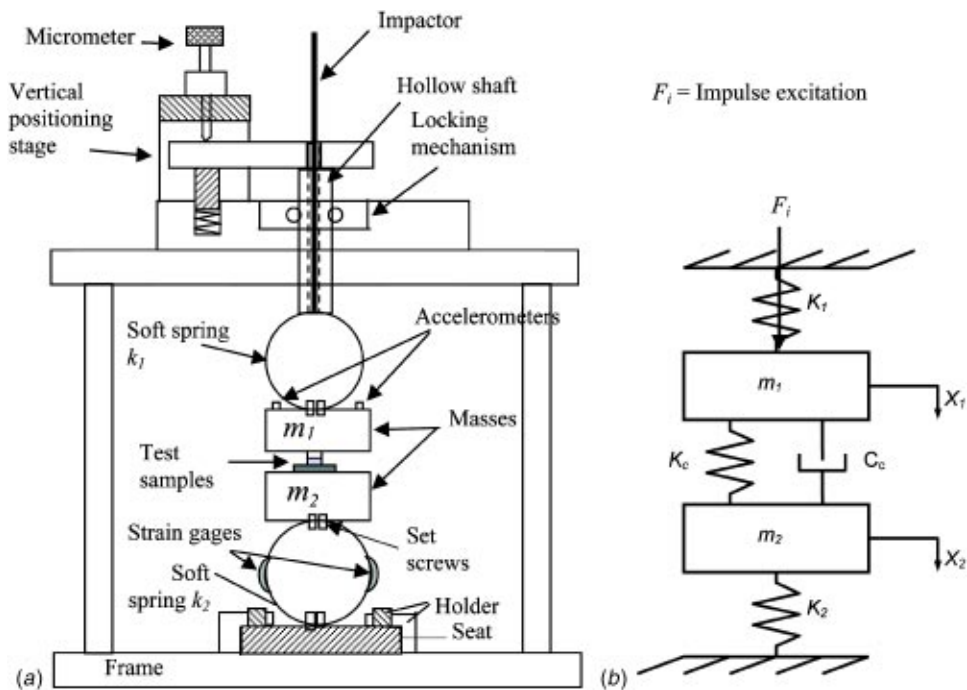


**Fig. 4 Meso-scale contact stiffness and damping tester (a) schematic, (b) system model**

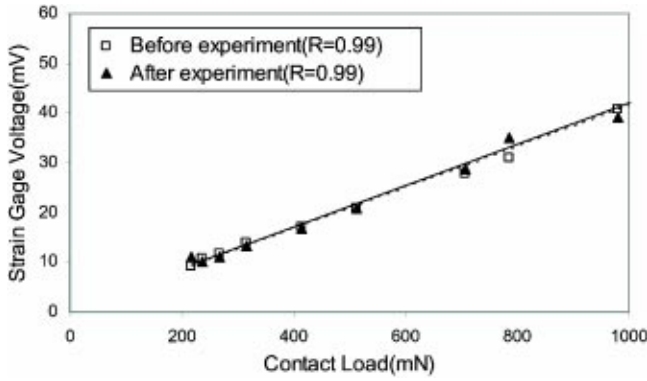
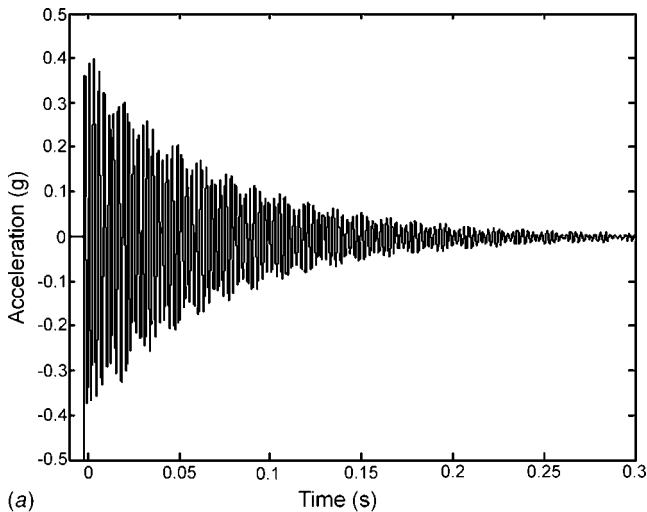


Fig. 5 Calibration of the strain gauge used for measuring the normal contact load

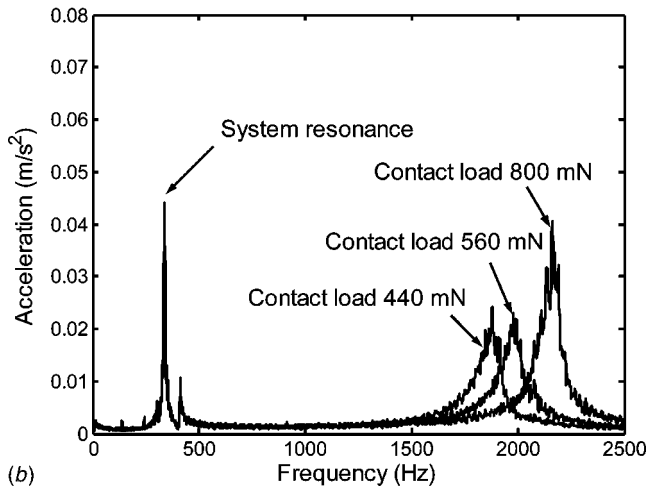
$$m_1 \ddot{x}_1 - c_c(\dot{x}_2 - \dot{x}_1) + k_c(x_1 - x_2) + k_1 x_1 = m_1 g \quad (9a)$$

$$m_2 \ddot{x}_2 + c_c(\dot{x}_2 - \dot{x}_1) - k_c(x_1 - x_2) + k_2 x_2 = m_2 g \quad (9b)$$

The characteristic equation is obtained as



(a)



(b)

Fig. 6 (a) Typical acceleration signal, (b) average spectra for rough flat surfaces contact with three different contact loads

$$\begin{vmatrix} -m_1 \omega^2 + j c_c \omega + k_c + k_1 & -j c_c \omega - k_c \\ -j c_c \omega - k_c & -m_2 \omega^2 + j c_c \omega + k_c + k_2 \end{vmatrix} = 0 \quad (10)$$

Solving for the contact stiffness, its value is a complex number and is given by

$$k_c = \frac{m_1 m_2 \omega^4 - (m_1 k_2 + m_2 k_1) \omega^2 + k_1 k_2}{(m_1 + m_2) \omega^2 - (k_1 + k_2)} - j c_c \omega \quad (11)$$

In the presence of contact damping, the root of the characteristic equation  $\omega$  is a complex number. Physically, it means that there is some signal decay because of the presence of damping. Since the effect of damping on contact stiffness is small, one is primarily interested on the absolute value of  $k_c$ . In the model considered in this work, the effect of contact damping on the calculation of  $k_c$  is ignored, and the contact stiffness is simply taken as the magnitude of Eq. (11), i.e., ignoring the imaginary part.

As described earlier, based on the acceleration signal from a typical impact experiment, one can readily extract the resonance frequencies, i.e.,  $\omega_1$ ,  $\omega_2$ , and the contact damping ratios. In this work, the Eigensystem Realization Algorithm (ERA) [22] method is used to extract the contact resonances and damping ratios directly from the acceleration measurements. ERA is time-domain realization technique based on a least-squares fit using a singular value decomposition to determine the model order. Note that other methods, such as spectrum analysis, were also used in this work to extract the resonant frequencies, and the results agree with the ERA results. According to Eq. (11), substitution of any one of the two resonances ( $\omega_1, \omega_2$ ) will give the contact stiffness. However, since  $\omega_1$  is almost unchanged with increasing contact load, whereas  $\omega_2$  strongly depend on the contact load, it is preferable to use  $\omega_2$ , in which is done in this work.

## 4 Experimental Results and Discussion

**4.1 Hertzian Contact.** In these experiments, a 1.59 mm (1/16 in.) diameter stainless steel sphere is used to contact a nominally flat stainless steel surface. The material and surface roughness parameters are shown in Table 2. The roughness parameters were extracted from 1-mm-long profilometric scans. Since both the flat and spherical samples possess roughness, the theoretical contact stiffness calculation is obtained from the Hertzian equation with roughness i.e., Eq. (3).

Before each experiment, the samples were cleaned using an ultrasonic cleaner and immersed in acetone, followed with propyl alcohol rinsing and drying with hot dry air. For rigidity, the sphere was pressed fit in a smaller hole on the flat sample, with the use of a minute amount of a rigid adhesive, and the flat samples were attached to the tube springs using set screws. To perform an experiment, the spherical sample was advanced downwards via a micrometer with 1  $\mu$ m resolution. The normal load was monitored from the strain gauge readout. Once the desired normal contact load was obtained, the upper system holding the sphere was locked in place to eliminate the compliance and the presence of any nonlinearity in the micrometer. Then, using the small impactor, a small impact was applied on the back side of the sample holding the sphere and the accelerations were digitally recorded on a computer for further processing. Analog filters were used to bandpass filter the acceleration signals from 10 Hz to 10 kHz, and the sampling rate was set at 25 kHz. Typical acceleration signals are as shown in Fig. 6(a) and average spectra in Fig. 6(b). The spectrum contains two peaks, the lower one associated with the compliant tube springs and the higher one with the contact resonance. The frequencies  $\omega_1$ ,  $\omega_2$ , and contact damping ratio  $\zeta_c$  were extracted directly from the acceleration signals using ERA. The contact stiffness  $k_c$  was then calculated using Eq. (11).

The experiments were performed under different loads ranging from 70 to 1000 mN. At each contact load, eight impact experiments were performed and averaged to reduce noise effects. In

**Table 3 Contact resonance values at different contact loads, Hertzian contact—system resonance is constant at all loads,  $\omega_1=281$  Hz**

Contact load (mN)	73.6	147.2	220.7	245.3	392.4	490.5	735.8	981.0
Contact resonance $\omega_2$ (Hz)	598	632	716	733	812	854	898	955

this range, the strain gauge has a good sensitivity and linearity. The data show that the system resonance is fixed at around 281 Hz and the contact resonance increases with increasing contact load as shown in Table 3. Specifically the contact resonance changes from 598 to 981 Hz when the contact load is 73.5 and 981 mN, respectively. Using Eq. (11), the calculated contact stiffness and using ERA the extracted contact damping values are shown in Fig. 7 with “box and whisker” plots under different levels of contact load. The box has lines corresponding to values at the lower quartile, median, and upper quartile values and the whiskers are lines extending from each end of the box to show the extent of the rest of the data. Outliers are data with values beyond the ends of the whiskers and if there are no data outside the whisker, a dot is placed at the bottom whisker. Clearly, the statistical variation of the data at each contact load is very small except for the contact damping ratio under light load. Specifically, the variation for the contact stiffness is typically less than 2.6% of the average value for eight tests. For the contact damping the variation is typically less than 11.1% of the average value for eight tests. Examining Fig. 7(a) which shows both the experimental and theoretical contact stiffness values, one observes that the measured values agree well with the theoretical values based on Hertzian theory. Spe-

cially, the experimental values fall between the theoretical Hertzian contact stiffness values for smooth surfaces and the rough Hertzian simulation results. As expected from Hertzian theory, the contact stiffness is nonlinear and behaves as a stiffening spring. The difference between the experimental and theoretical (rough results), especially at higher loads, is due to the assumption that roughness decreases the Hertzian contact stiffness by a factor of 3, which is only approximate. As explained in Sec. 2.1., according to Ref. [19], this factor is only applicable at lower loads. Nevertheless, the measured results are consistent with models from the literature.

Based on the above-mentioned Hertzian results, it is confirmed that the proposed meso scale contact stiffness and damping tester is capable of measuring the interfacial properties reliably at a normal load range from about 100 to 1000 mN. Note also that the above-mentioned experimental contact stiffness values were also confirmed using spectrum analysis of the acceleration signals.

Using ERA analysis, the contact damping ratio at each contact load is calculated and is shown in Fig. 7(b). It is seen that at light loads, the contact damping is much higher than that at higher loads—specifically, at 100 mN,  $\zeta_c=17\%$  and at 1000 mN,  $\zeta_c=3\%$ . It is postulated that the reason for the difference is due to the presence of micro-slip at the interface during the impact (or indentation) process, in agreement with Ref. [23]. At higher loads, the interface is more constrained, resulting in less micro-slip and thus smaller damping. Also, notice that the contact damping decreases quickly with increasing load at lighter loads, but when the load reaches some level, there is no obvious contact damping change with further load increase. To confirm that indeed the damping remains constant at even higher loads, several impact experiments were performed at even higher loads up to 3 N and it was found that the contact damping is nearly unchanged. For example, the damping ratio for 2.5 N is about the same as the one at 1 N, i.e.,  $\zeta_c \approx 3\% - 4\%$ . The contact damping ratio decrease with increasing contact load has also been reported in the literature. For example, in Ref. [24] it was reported that lower clamping forces during machining, result in improved dimensional precision, due to higher contact damping in the tangential direction. Such findings are somewhat counterintuitive, as one usually expects that increasing clamping forces will result in less work-piece movement and thus improved dimensional accuracy.

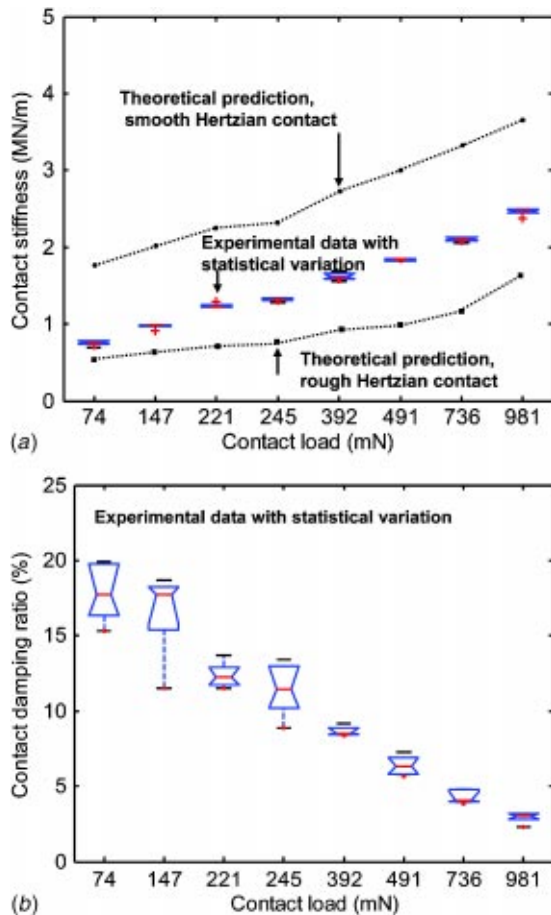


**Fig. 7 Hertzian contact: (a) contact stiffness; (b) contact damping ratio versus contact load**

## 4.2 Flat Rough Surfaces in Contact

**4.2.1 Unlubricated (Dry) Conditions.** For these experiments, typical stainless steel (type 17/4PH) flat samples were used to obtain the contact stiffness and damping. The material and roughness parameters are shown in Table 4. Both samples were machine ground and then polished with 600-grit paper to obtain the desirable roughness properties. The nominal contact area is  $1.824 \text{ mm}^2$ .

The procedure for performing the experiments at different normal loads is the same as described earlier for the Hertzian contact. Particular emphasis is given to ensure that the two flat samples are aligned properly with the contact area equaling the nominal contact area of the samples. From the acceleration data, the resonant frequencies were extracted using the ERA method (also confirmed using spectrum method) and as expected, the first resonance is fixed at around 356 Hz and the values of the second resonance at different contact loads are listed in Table 5. In this case the change in the contact resonance with normal load is much larger than the Hertzian case (Table 3), changing from 1410 Hz at 264.9 mN to

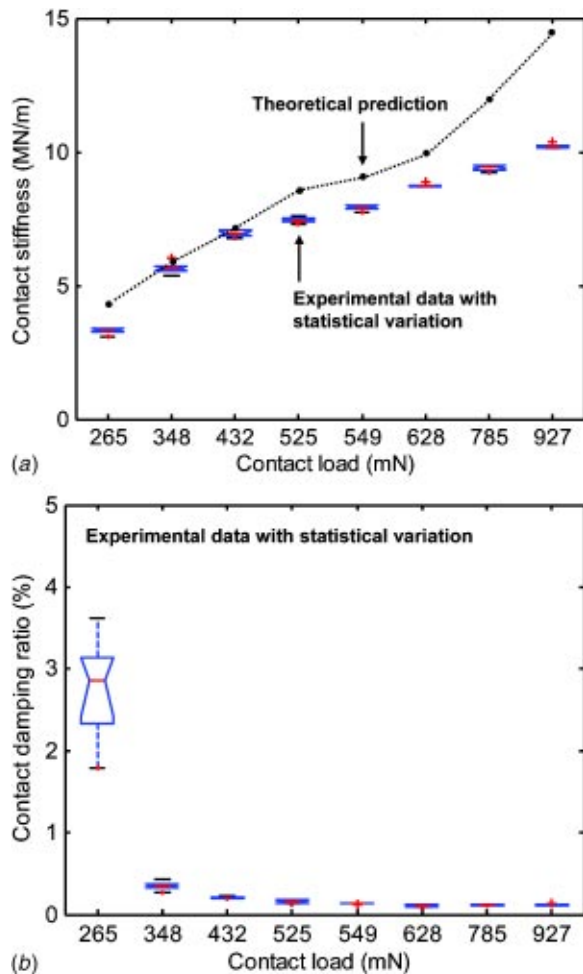
**Table 4 Material and roughness parameters for contacting flat rough surfaces**

	Individual surface parameters					Combined interface parameters			
	$E$ (GPa)	$H$ (GPa)	$R_q$ ( $\mu\text{m}$ )	$R_s$ ( $\mu\text{m}$ )	$\eta$ ( $/\mu\text{m}^2$ )	$E^*$ (GPa)	$R_s$ ( $\mu\text{m}$ )	$\eta$ ( $/\mu\text{m}^2$ )	$R_q$ ( $\mu\text{m}$ )
Sample 1	192.92	2.96	0.167	3.555	0.122	105.3	2.402	0.1256	0.189
Sample 2	192.92	2.96	0.088	7.409	0.144				

**Table 5 Contact resonance values at different contact loads, flat rough surfaces—system resonance is constant at all loads,  $\omega_1=356$  Hz**

Contact load (mN)	264.9	348.3	431.6	524.8	549.4	627.8	784.8	927.0
Contact resonance $\omega_2$ (Hz)	1410	1701	1855	1925	1979	2079	2146	2234

2234 Hz at 927 mN. Using  $\omega_2$  in Eq. (11), the experimental contact stiffness values at each load are obtained. Based on rough surface contact theory as described in Sec. 2.2.2, the theoretical contact stiffness values are also calculated using the CEB elastic contact model. The experimental and theoretical contact stiffnesses versus contact load are shown in Fig. 8(a). Again, the experimental data are plotted showing their statistical variation using “box and whisker” plots under different levels of contact load.

**Fig. 8 Flat rough contacting surfaces: (a) contact stiffness; (b) contact damping ratio versus contact load**

Referring to Fig. 8(a), as expected the values of the contact stiffness are higher than the Hertzian contact (see Fig. 7), and they also nonlinearly increase with load. Specifically, at 200 mN,  $k_c = 3$  MN/m and at 1000 mN,  $k_c = 10$  MN/m. At lower loads from 200 to 600 mN, the experimental results agree with the theoretical predictions very well. At higher loads the experimental values are lower than the theoretical predictions, even though they are still similar. A reason for this difference is that at lower loads, the nonlinearity is not as significant as at high loads. A strong nonlinearity will cause a large frequency distortion and thus the resonance frequency will be significantly lower than the actual value.

The experimental contact damping behavior is similar to the Hertzian case, i.e., it decreases with increasing load. However, compared to the Hertzian contact, the contact damping in the case for the flat rough surfaces is significantly lower as shown in Fig. 8(b). Notice that in this case, the statistical variation of the data is again very small as shown in the figure, except for the lowest load of 265 mN, which is significant. Specifically, the contact damping varies from as high as 2.8% at low loads to only 0.16% at loads higher than 500 mN. The lower damping can be explained by the fact that (a) the flat surfaces are smoother than the Hertzian surfaces, and (b) according to Ref. [23], the ratio of slip zone size to the contact zone size is the same for spherical (Hertzian) and flat (punch) contacts. However, the slip zone for the Hertzian contact always remains a “curved surface,” resulting in a larger actual slip area than the flat surface. Thus the Hertzian contacts have larger damping compared to flat surfaces contact. This smaller damping ratio for flat rough surfaces in contact is very important in practical applications. It suggests that Hertzian contacts as well as rougher contacting interfaces will lead to higher contact damping, especially at lower contact loads.

**4.2.2 Effect of Boundary Lubricant and Wear Debris.** The above-presented experiments were performed under the simpler conditions of unlubricated, or dry contacts. Practically, many contacts contain small amounts of liquid lubricant or grease, and wear particles resulting for example from friction or fretting wear. In this work, experiments in the presence of boundary lubrication and wear debris were also performed to investigate their effect on the contact stiffness and damping. The samples used here were the same as for the dry experiments (see Table 4). After cleaning the samples with acetone and alcohol, in the case of the boundary lubricated experiments, a very small amount of 2 mg of a commercially available polyolester (POE) lubricant was added to the contact before testing. The small amount of lubricant simulates boundary and mixed lubrication conditions. In the case of the wear debris experiments, after sample preparation the surfaces were manually rubbed against each other at a normal load of approximately 5 N and in a reciprocating motion at a total of 100 times. Examination under the microscope confirmed the presence of minute wear particles.

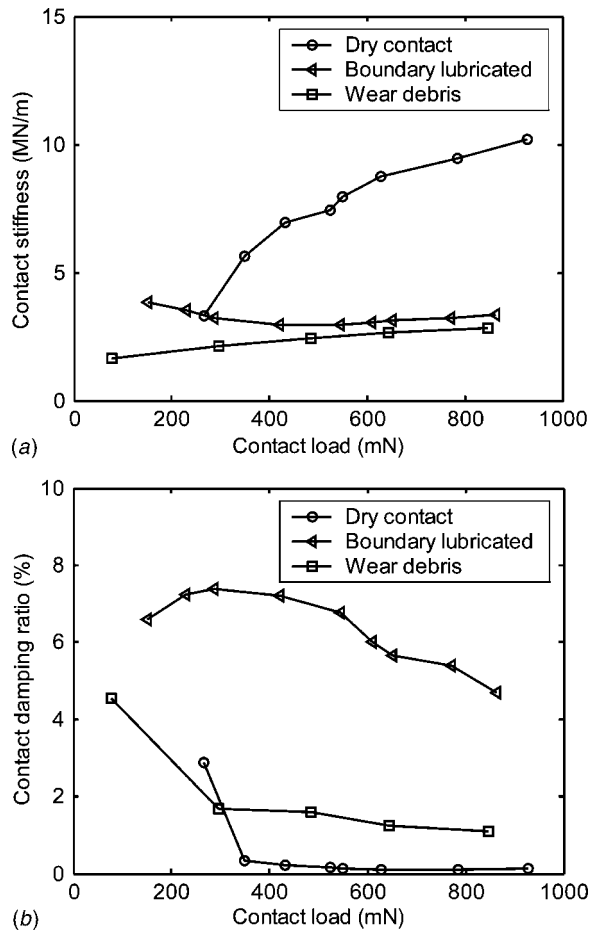


**Fig. 9 Experimental measurements for flat rough contacting surfaces under different conditions: (a) contact stiffness; (b) contact damping ratio versus contact load**

The results from these experiments are depicted in Fig. 9. Referring to Fig. 9(a), both the presence of lubricant and wear debris will significantly decrease the contact stiffness. Specifically at 500 mN,  $k_c = 2.45, 2.97,$  and  $7.31$  MN/m for wear debris, boundary lubricated, and dry conditions, respectively. The significance of this finding in engineering applications is that the presence of small amounts of lubricant or wear debris will significantly decrease the contact stiffness at the interface.

The effect of boundary lubricant and wear debris on damping is shown in Fig. 9(b). The lubricant increases damping significantly, whereas the presence of wear debris slightly increases the damping. At 500 mN,  $\zeta_c = 0.18\%, 1.60\%,$  and  $6.85\%$  for dry, wear debris, and boundary lubricated conditions, respectively. As with the contact stiffness findings, the significance of the contact damping findings in practical engineering applications can be seen, for example, by adding small amounts of lubricant at a joint, thus increasing significantly its damping and energy dissipation properties.

## 5 Conclusions

A simple and straightforward experimental method was developed to measure the contact stiffness and contact damping of realistic spherical Hertzian and rough flat surfaces in contact. The tester is capable of testing lightly loaded interfaces with normal loads ranging from 100 to 1000 mN. It is found that contact stiffness is lower for Hertzian contacts compared to flat surfaces in contact, which is in agreement with theoretical predictions. Also, with both Hertzian and flat surfaces, the effect of surface roughness is very important in decreasing the contact stiffness by sev-

eral orders of magnitude, compared to infinitely smooth deformable solid surfaces. Furthermore, in both Hertzian and flat surfaces the experimentally measured contact stiffness values agree well with theoretical calculations based on rough Hertzian and rough flat contacting surfaces. In both Hertzian and flat surfaces, the contact stiffness nonlinearly increases with increasing contact load, behaving as a nonlinear stiffening spring. On the other hand, contact damping decreases with increasing contact load. Compared to rough flat dry surfaces in contact, Hertzian dry contacts have significantly larger damping. This suggests that Hertzian contacts are more efficient than flat contacting surfaces in the design of fasteners and other interfaces since higher damping usually provides improved dynamic system performance. Lastly, the effects of lubricant and wear debris were investigated and it was found that both lubricant and wear debris significantly decrease the contact stiffness, however, only the lubricant significantly increases the contact damping.

## Acknowledgments

This research was supported by the Research Board of the University of Illinois at Urbana Champaign and the National Science Foundation under Grant No. CMS-0239232 and the supervision of program officer Dr. Jorn Larsen-Basse. The authors gratefully acknowledge these supports.

## Nomenclature

- $a$  = contact radius for infinitely smooth flat surfaces
- $A_n$  = nominal contact area
- $c$  = constant coefficient in Eq. (7)
- $c_c$  = contact damping coefficient
- $d$  = mean normal separation between rough surfaces
- $d_{th}$  = thickness of solid infinity smooth surface
- $E^*$  = composite elastic modulus
- $g$  = acceleration due to gravity
- $H$  = hardness of softer material
- $k_1, k_2$  = stiffness of tube springs
- $k_c$  = flat rough surface contact stiffness
- $k_{CH}$  = Hertzian smooth contact stiffness
- $k_{CHR}$  = Hertzian rough contact stiffness
- $K$  = material constant in Eq. (6),  $K = 0.454 + 0.41\nu_2$
- $m_1, m_2$  = masses of tester blocks
- $P$  = normal contact force
- $R$  = sphere radius (equivalent:  $R^{-1} = R_1^{-1} + R_2^{-1}$ )
- $R_a$  = Center line average roughness
- $R_q$  = rms roughness of asperity heights
- $R_s$  = average radius of asperities
- $x_1, x_2$  = normal displacements of mass blocks
- $\dot{x}_1, \dot{x}_2$  = normal velocities of mass blocks
- $\ddot{x}_1, \ddot{x}_2$  = normal accelerations of mass blocks
- $z$  = asperity height
- $\beta$  = roughness parameter,  $\eta R_s R_q$
- $\Delta$  = surface normal approach
- $\zeta_c$  = contact damping ratio
- $\eta$  = areal density of asperities
- $\lambda$  = constant coefficient in Eq. (7)
- $\nu$  = Poisson's ratios
- $\phi$  = distribution function of asperity heights
- $\omega$  = resonance frequency
- $\omega_1$  = system resonance
- $\omega_2$  = contact resonance
- $\Omega$  = asperity interference
- $\Omega_c$  = critical asperity interference

## References

- [1] Maekawa, H., and Komoriya K., 2001, "Development of a Micro Transfer Arm for a Microfactory," Proceedings of the 2001 IEEE International Conference on Robotics & Automation, pp. 1444–1451.

- [2] Armstrong-Hélouvy, B., 1991, *Control of Machines with Friction*, Kluwer Academic, Boston.
- [3] Maruyama, T., Sanda, S., Sato, M., and Uchiyama, T., 1990, "Hand-eye System with Three-Dimensional Vision and Microgripper for Handling Flexible Wires," *Mach. Vision Appl.*, **3**, pp. 189–199.
- [4] Bhushan, B., 1996, *Tribology and Mechanics of Magnetic Storage Devices*, 2nd ed. Springer, New York.
- [5] Rohde, S. M., 1980, "A Mixed Friction Model for Dynamically Loaded Contacts with Application to Piston Ring Lubrication," *Surface Roughness Effects in Hydrodynamic and Mixed Lubrication*, ASME-The Lubrication Division, pp. 29–50.
- [6] Johnson, K. L., Greenwood, J. A., and Poon, S. Y., 1972, "A Simple Theory of Asperity Contact in Elastohydrodynamic Lubrication," *Wear*, **19**, pp. 91–108.
- [7] Johnson, K. L. 1985, *Contact Mechanics*, Cambridge University Press, London.
- [8] Greenwood, J. A., and Williamson, J. P. B., 1966, "Contact of Nominally Flat Surfaces," *Proc. R. Soc. London, Ser. A*, **295**, pp. 300–319.
- [9] Polycarpou, A. A., and Soom, A., 1995, "Boundary and Mixed Friction in the Presence of Dynamic Normal Loads. I. System Model," *ASME J. Tribol.*, **117**, pp. 255–260.
- [10] Song, Y., Hartwigsen, C. J., Bergman, L. A. and Vakakis, A. F., 2004, "Simulation of Dynamics of Beam Structures with Bolted Joints Using Adjusted Iwan Beam Elements," *J. Sound Vib.*, **273**(1-2), pp. 249–276.
- [11] Serpe, C. I., 1999, "The Role of Contact Compliance in the Deformation, Wear and Elastic Stability of Metallic Sliding Rings: Experiments and Computational Analysis," Ph.D. Dissertation, State University of New York at Buffalo, NY.
- [12] Hess, D. P., and Wagh, N. J., 1995, "Evaluating Surface Roughness From Contact Vibrations," *ASME J. Tribol.*, **117**, pp. 60–64.
- [13] Robinson, A. M., Drinkwater, B. W., Dwyer-Joyce, R. S., and Payne, J. F. B., 2001, "Measurement of the Stiffness of Joints in Graphite Brick Assembly," *Proc. Inst. Mech. Eng., Part C: J. Mech. Eng. Sci.*, **215**, pp. 167–178.
- [14] Dwyer-Joyce, R. S., Drinkwater, B. W., and Quinn, A. M., 2001, "The Use of Ultrasound in the Investigation of Rough Surface Interfaces," *ASME J. Tribol.*, **123**, pp. 8–16.
- [15] Syed Asif, S. A., Wahl, K. J., Colton, R. J., and Warren, O. L., 2001, "Quantitative Imaging of Nanoscale Mechanical Properties Using Hybrid Nanoindentation and Force Modulation," *J. Appl. Phys.*, **90**, pp. 1192–1200.
- [16] Gao, H., and Wu, T., 1993, "A Note on the Elastic Contact Stiffness of a Layered Medium," *Mater. Res. Soc. Symp. Proc.*, **8**, pp. 3229–3232.
- [17] Li, X., and Bhushan, B., 2000, "Development of Continuous Stiffness Measurement Technique for Composite Magnetic Tapes," *Scr. Mater.*, **42**, pp. 929–935.
- [18] Williams, J. A., 1994, *Engineering Tribology*, Oxford University Press, New York.
- [19] Greenwood, J. A., and Tripp, J. H., 1967, "The Elastic Contact of Rough Spheres" *ASME J. Appl. Mech.*, **34E**, pp. 153–159.
- [20] Chang, W. R., Etsion, I., and Bogoy, D. B., 1987, "An Elastic-Plastic Model for the Contact of Rough Surfaces," *ASME J. Tribol.*, **109**, pp. 257–263.
- [21] Polycarpou, A. A., and Etsion, I., 1999, "Analytical Approximations in Modeling Contacting Rough Surfaces," *ASME J. Tribol.*, **121**, pp. 234–239.
- [22] Inman, D. J., 1996, *Engineering Vibration*, Prentice-Hall, Englewood Cliffs, NJ.
- [23] Spence, D. A., 1975, "The Hertz contact problem with finite friction," *J. Elast.*, **5**, pp. 297–319.
- [24] Fang, B., Devor, R. E., and Kapoor, S. G., 2002, "Influence of Friction Damping on Workpiece-Fixture System Dynamics and Machining Stability," *ASME J. Manuf. Sci. Eng.*, **124**, pp. 226–233.